

How Fast Do Fluids Squeeze through Microscopic Single-File Pores?

Tom Chou

DAMTP, Cambridge University, Cambridge CB3 9EW, England

(Received 18 August 1997)

A one dimensional symmetric exclusion model is used to study pressure and osmosis driven flows through molecular-sized channels, such as biological membrane channels and zeolite pores. Analytic expressions are found for the steady-state flow as a function of pore radius, pore energetics, reservoir temperature, driving force, and internal defects. We find a flux maximum as a function of particle-pore interactions: This, and other nonlinear dependences suggest numerous diagnostic experiments for biological and zeolitic systems. [S0031-9007(97)05268-X]

PACS numbers: 47.55.Mh, 05.60.+w

The answer to the title question is tremendously important for modeling biological and industrial processes, and has received recent attention with experimental (NMR) and theoretical findings that motions of interacting (due to excluded volume) tracer particles in molecular-sized pores are governed by subdiffusive dynamics [1]. Biological examples include integral membranes channels that are molecular sized and are specific to water and ion transport which participate in hydrostatic or osmotic pressure controlled cellular volume regulation [2]. Man-made materials such as zeolites and carbon nanotubes may also contain many microscopic, nearly single-file channels that can selectively absorb fluids. This size specificity can be exploited in the separation of linear and branched chain alkanes, where the zeolite acts as a sponge, absorbing only the desired species [3]. Confining particles in zeolite pores can also serve to catalyze reactions: How fast can one get reagents into micropores and the products out?

Therefore, the design and manufacture of porous materials [4] is an economically motivated area of research, and numerous molecular dynamics (MD) studies have been performed on a variety of specific systems [5]. Anomalies in numerically computed (MD) “diffusion” constants have been found [6]. However, numerical simulations neither access the long time scales required to study steady state flow, nor offer a unifying physical picture of the parameters important for transport. To obtain reasonable flow rates using MD, artificial external forces such as gravity are often imposed [7]; in 1D systems such external forces can yield qualitatively different behavior (such as shock profiles) from osmosis and pressure driven flow [8], which occur in the absence of such intrinsic forces.

A model that physically describes transport and how flows depend on microscopic molecular parameters and macroscopic thermodynamic constraints would serve as a useful benchmark in more sophisticated models and complement more detailed MD simulations. Consider the molecular-sized pore shown in Fig. 1, with particles driven from (L) to (R) either by osmotic “pressure” $\Delta\Pi$, or by hydrostatic pressure ΔP . The pore is divided into i sections of length ℓ each with possible activation energies between bulk and pore particles shown. Entrance

(exit) rates at the left and right boundary sites are defined by $\alpha(\gamma)$ and $\delta(\beta)$, respectively. Here, αdt and δdt are the probabilities for pore entry in time dt only if the occupations ($\tau_i = 0$ or 1) $\tau_1 = 0$ and $\tau_N = 0$, respectively. The probability per unit time a randomly picked interior particle within section i moves to the right (left) is $p(q)$ only if the site to the right (left) is unoccupied. The implicit random particle hop updating is valid when long wavelength collective modes are irrelevant. The assumption of no pass pores is accurate even for pore diameters $\sim(2-3)\times$ particle diameters since overtaking requires a restricted subset of geometries and will be statistically rare. Even when overtaking occurs, interchange between particles at sites i and $i+1$ does not contribute to net flux as long as the average number of particles in a cylindrical section of length ℓ is <1 . Consider the instantaneous number flux between sections i and $i+1$,

$$\begin{aligned} J_i(t) &= p\tau_i(t)[1 - \tau_{i+1}(t)] - q\tau_{i+1}(t)[1 - \tau_i(t)] \\ &\equiv p[\tau_i(t) - \tau_{i+1}(t)] + \epsilon\tau_{i+1}(t) - \epsilon\tau_i(t)\tau_{i+1}(t). \end{aligned} \quad (1)$$

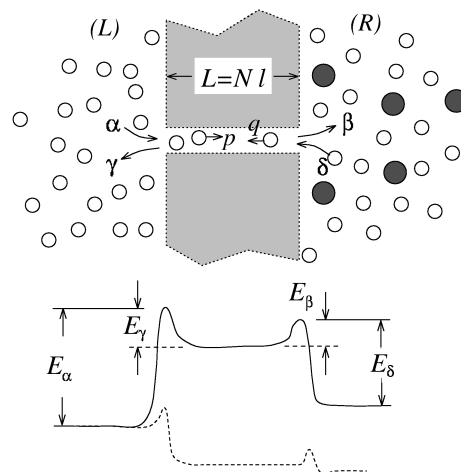


FIG. 1. Schematic of osmosis and pressure driven flow through membrane pores separating infinite reservoirs (L) and (R). The coefficients α , β , γ , and δ are conditional solvent entrance and exit probabilities at pore ends.

Although much attention has focused on the asymmetric exclusion model ($\epsilon \equiv p - q \neq 0$), particularly in the thermodynamic limit, where some exact results are known [8], the symmetric exclusion model ($\epsilon = 0$) is valid in the absence of external electric or gravitational forces. Locally, particles in microscopic pores that are weakly self-attracting are as likely to move to the left or right *if* both left and right adjacent sites are unoccupied. However, a gradient in τ_i yields biased diffusion and a net flux. Related models have been proposed for one

lane traffic flow [9]; however, these are highly asymmetric ($\epsilon = p$ since drivers rarely reverse) and include random p and acceleration effects.

Linearity of $J(t)$ when $\epsilon = 0$ renders the mean-field steady state current J found from time averaging Eq. (1) exact. Steady state particle conservation along the pore length results in a linear density profile $J = p(\tau_1 - \tau_N)/(N - 1)$; this, along with the steady state boundary conditions $J_0 = J = \alpha(1 - \tau_1) - \gamma\tau_1$ and $J_N = J = \beta\tau_N - \delta(1 - \tau_N)$, determine the steady state particle number flux

$$J(N) = \frac{p(\alpha\beta - \gamma\delta)}{(N - 1)(\alpha + \gamma)(\beta + \delta) + p(\alpha + \beta + \gamma + \delta)}. \quad (2)$$

The kinetic parameters $\{\mu\} \equiv (\alpha, \beta, \gamma, \delta)$ are related to the *relative* enthalpies of activation E_μ between pore and bath particles. We assume local thermodynamic equilibrium (LTE), valid when collision times \ll mean transport times. In liquid phase osmosis across single biological pores where $J \leq 10^9$ /s, typical pore diameters and interparticle spacings $\lambda \sim 5 \text{ \AA}$, and ambient thermal velocities $v_T \approx 4 \times 10^4 \text{ cm/s}$, yield collision times $t_{\text{coll}} \approx \lambda/v_T \approx 1 \text{ ps} \ll J^{-1}$. Therefore, particles suffer $O(10^3)$ collisions before they are osmotically transported, sufficient for (LTE). As an illustrative example, we consider an axisymmetric right cylindrical pore ($\gamma = \beta$), where $\{\mu\}$ in LTE will be defined by simple transport theory,

$$\begin{aligned} p &\approx (v_T/\ell) \exp(-E_p/k_B T), \\ \beta &\approx (v_T/\ell) \exp(-E_\beta/k_B T), \\ \alpha[\delta] &\equiv \alpha_0[\delta_0] \exp(-E_{\alpha[\delta]}/k_B T) \\ &\approx \frac{1}{4} n_{L[R]} v_T (\pi r_p^2) \exp(-E_{\alpha[\delta]}/k_B T), \end{aligned} \quad (3)$$

where $v_T \sim \sqrt{k_B T/m}$ is the thermal velocity, ℓ is chosen to be the minimum statistical spacing between pore

particles (estimated, for example, for each $\{\mu\}$ from a 1D Tonk's gas [10]), and $n_{L[R]}$ is the number density in the left [right] reservoir. The internal hopping rate p given by (3) represents a ballistic travel time over the distance $\ell \approx a$, weighted by an energetic binding E_p . A larger choice for ℓ can be made if $(\ell/a)\tau_i < 1$ and with p appropriately rescaled and entropic factors included for $\{\mu\}$ (the E_μ are then effective free energies); this is useful in multiple species models where steady state flows for long pores cannot be obtained analytically [11]. Note that for $\ell \gg a$, *local* free diffusive transport described by $p \approx \ell^{-2}$ may obtain. Since we explore considerable variations in $\{\mu\}$, we choose $\ell \sim a$ (approximately a repulsive hard core diameter) and E_μ represent enthalpies determined entirely by molecular potentials. Thus, $E_\alpha(r \leq r_p) - E_\alpha(0) \lesssim k_B T$ [where $E_\alpha(r = 0) \equiv E_\alpha$] defines an effective pore radius r_p . For pores that repel particles (top curve in Fig. 1) and have negligible activation energies (E_β, E_p), $p/\beta \sim O(1)$.

Upon normalizing (denoted by an overbar) all quantities by β (such that $\bar{J} \equiv J/\beta = 1$ is the maximum flow rate possible, when $\tau_N = 1$, and $\bar{\alpha}$ defines a solvent-pore affinity, or binding constant),

$$\bar{J}(N) = \frac{\bar{\alpha} \bar{p} \Delta}{(N - 1)(\bar{\alpha} + 1)(\bar{\alpha} + 1 - \bar{\alpha} \Delta) + \bar{p}(2\bar{\alpha} + 2 - \bar{\alpha} \Delta)}, \quad (4)$$

where

$$\Delta = \frac{\alpha - \delta}{\alpha} \approx 1 - e^{\Delta E/k_B T} + \frac{\Delta n_{\text{solute}}}{n_L} e^{\Delta E/k_B T} \quad (5)$$

and $\Delta E \equiv E_\alpha - E_\delta(P_R - P_L)$. Equation (5) represents differences in number density and/or enthalpies between (R) and (L) and along with (4) determine the flow through symmetric pores. Under isobaric conditions (pure osmosis), $\Delta E = 0$; in nearly ideal gases, $(\partial \Delta E / \partial P_R)_T \approx 0$, while hydrostatically driven flows of liquids is described by $(\partial n_R / \partial P)_T \approx 0$. In the first two cases, the J results predominately from an increased permeable particle density in one of the reservoirs over the other, while pressure driven flows of liquids result mainly from the relative reduction of pore entrance activation energies brought about

by hydrostatic compression. First consider $\Delta = 0.02$, which corresponds to an osmotic pressure in aqueous solution of $\Delta \Pi \approx 25 \text{ atm}$ or a hydrostatic pressure difference of $\Delta P \approx 0.025 \text{ atm}$ of gas at STP. Using the Maxwell relationship for particle volume, $-(\partial \Delta E / \partial P_R)_T \approx \bar{v}$, we find $\Delta = 0.02$ also corresponds to $P_R - P_L \approx 25 \text{ atm}$ in pressure driven flow of water at 300 K.

Large values of $\bar{\alpha}$ represent pores which are attractive to the solvent (for example, the dashed energy landscape in Fig. 1). When $\bar{\alpha} \Delta / (\bar{\alpha} + 1)$ is negligible, flows are essentially linear in Δ and defined by hydraulic or osmotic permeabilities, $J \cong L_p \Delta P$ or $J \cong P_{os} \Delta \Pi$. Although L_p and P_{os} is often interpreted using *macroscopic* fluid mechanics [2], a microscopic description arises here. In

the limit $\bar{p} \gg (\bar{\alpha} + 1)N$, rate limiting steps involve pore entrance or exit. Linearizing (4) and (5), we find

$$L_p = \frac{\alpha}{2(\bar{\alpha} + 1)k_B T} \left(\frac{\partial \Delta E}{\partial P_R} \right)_T \quad (6)$$

for pressure driven flow of dense liquids. The temperature dependence of L_p will be determined by $-E_\beta/k_B T [-E_\alpha/k_B T]$ for $\bar{\alpha} \gg 1$ [$\bar{\alpha} \ll 1$] if the thermal coefficient of expansion of the fluid is small. When $\bar{p} \ll (\bar{\alpha} + 1)N$,

$$L_p = \frac{\alpha \bar{q}}{(N - 1)(\bar{\alpha} + 1)^2 k_B T} \left(\frac{\partial \Delta E}{\partial P_R} \right)_T, \quad (7)$$

which has a $(E_\alpha - E_\beta - E_p)/k_B T [(E_\beta - E_\alpha - E_p)/k_B T]$ Arrhenius temperature dependence for $\bar{\alpha} \gg 1$ [$\bar{\alpha} \ll 1$]. In the limit where (7) holds, the rate limiting steps are particle motions within the pore interior. Ideal gas limit expressions for $L_p [P_{os}]$ are found by replacing $(\partial \Delta E / \partial P_R)_T$ by $-n_L^{-1} [+n_L^{-1}]$ in the corresponding limits (6) and (7); the temperature dependences remain unchanged.

The solid curve in Fig. 2(a) shows $(1.5 \times 10^3) \times \bar{J}(N)$ [from Eq. (4)] for $\bar{p} = 1$, $\Delta = 0.02$ for various pore lengths $N \approx L/a$. We find a maximum \bar{J}^* at

$$\bar{\alpha}^* = \left[\frac{2\bar{p}_0 + (N - 1)}{(N - 1)(1 - \Delta)} \right]^{1/2} \quad (8)$$

for fixed $\bar{p} = \bar{p}_0$. The maximum at an intermediate affinity $\bar{\alpha}^*$ (and occupation τ_i) occurs because the pore is conducting a substantial number of particles, without being choked off by high τ_i . However, as the pore is made increasingly attractive, $E_\beta > 0$ must eventually increase, β diminishes, and $\bar{p} = p/\beta \propto \exp[(E_\beta - E_p)/k_B T]$. We will explicitly show, nevertheless, that the flux maximum at \bar{J}^* can persist. Assume no activation barriers at the pore mouths, i.e., $E_\beta[E_\alpha] = 0$ for $E_\alpha[E_\beta] > 0$, and

consider molecularly repelling pores where $0 < \bar{\alpha} < \bar{\alpha}_0$ ($E_\alpha > 0$, $E_\beta = 0$); here, $\bar{p} \approx \exp(-E_p/k_B T)$, independent of the pore energy level. As the pore is made attracting, \bar{p} will acquire $\exp(E_\beta/k_B T)$ behavior and can be defined as

$$\bar{p} = \bar{p}_0 \left[\frac{\bar{\alpha}}{\bar{\alpha}_0} \theta(\bar{\alpha} - \bar{\alpha}_0) + \theta(\bar{\alpha}_0 - \bar{\alpha}) \right], \quad (9)$$

where $\theta(x > 1) = 1$ is the Heaviside function indicating the value of α_0 when the pore first becomes molecularly attracting. Upon using (9), the current across infinitely attracting pores becomes $\bar{J}^\infty(N) = \bar{p}_0 \Delta / [\bar{\alpha}_0(N - 1)(1 - \Delta) + \bar{p}_0(2 - \Delta)]$, which can approach $\Delta/(2 - \Delta) > \bar{J}^*$. For $\bar{\alpha}_0 \gg \bar{\alpha}^*$, the maximum remains at $\bar{\alpha}^*$. However, when $\bar{\alpha}_0 \lesssim \bar{\alpha}^*$, $\bar{\alpha}$, $\bar{p} \approx \exp(E_\beta/k_B T)$, and the maximum in flux as a function of $\bar{\alpha}$ is preempted by a current which monotonically approaches \bar{J}^∞ . A high current may occur at $\bar{\alpha} \rightarrow \infty$ despite the high-pore occupancy due to an accompanying exponential increase in \bar{p} . High currents are more difficult to achieve as $\bar{\alpha}_0$ (as well as N) increases, because the onset of exponentially increasing \bar{p} is delayed.

The condition for $\bar{J}^\infty(N) < \bar{J}^*(N)$ (a maximum in \bar{J} remaining as pore well depth is increased) is determined by

$$\bar{\alpha}_0 > \bar{\alpha}^* + \frac{\bar{\alpha}^{*2}}{\bar{\alpha}^* + 1}. \quad (10)$$

Figure 2(b) compares the behavior of $10^4 \times J(5)$ using $\bar{p} = \bar{p}_0 = 0.1$ (solid curve) with that of $10^4 \times J(5)$ using Eq. (9) (broken lines). For $\Delta = 0.02$, the maximum at $\bar{\alpha}^* = \sqrt{15/14}$ is destroyed when (10) is satisfied, $\bar{\alpha}_0 \lesssim 1.562$. Estimating $\bar{\alpha}_0$ from (3) and $\Delta = 0.02$, $\bar{\alpha}_0 \ll \bar{\alpha}^*$ for gases, but can be $O(1)$ for liquids. Curve $P_0 P_1 P_4 P_3$ retains the maximum \bar{J}^* since $\bar{\alpha}_0 = 10^{0.75} > 1.562$, while $P_0 P_1 P_2$ corresponds to $\bar{\alpha}_0 = 10^{-0.25} < 1.562$ which gives a monotonic J as $\bar{\alpha} \rightarrow \infty$. Note that when a maximum persists and the $\bar{\alpha} \gg 1$ regime of (7) obtains, a curious $L_p \propto r_p^{-2}$ dependence arises.

According to (8), values of $\bar{\alpha}$ that give a maximal \bar{J}^* depend strongly on Δ ; thus, $\Delta \rightarrow 1$ can yield large $\bar{\alpha}^* \gg \bar{\alpha}_0$ where the maximum in flux is destroyed. At the maximum value $\Delta = 1$ [corresponding approximately to pure solute or vacuum in (R)], the maximum flux occurs when $\bar{p} \gg N$ and approaches $\bar{J}(\Delta = 1) \approx \bar{\alpha}/(\bar{\alpha} + 2)$. The smallest flux occurs when $\bar{p} \ll N$ and $\bar{\alpha} \ll 1$ as expected. The nonlinearity of $\bar{J}(\Delta)$ is important only when $\bar{\alpha} \gg 1$, as shown in Fig. 3, corresponding to a pore interior with high particle occupation, when particle exclusion nonidealities are most pronounced.

A possible experimental probe for the predicted behavior, particularly in artificial pores, is to use adiabatic ultrasonic driving of the fluid in (R) (so as to not affect $\bar{\alpha}$ which depends only on n_L) with frequency $\omega \ll J$ to enhance transport: Upon setting $\Delta(t) = \Delta_0 + \Delta_1 \cos \omega t$

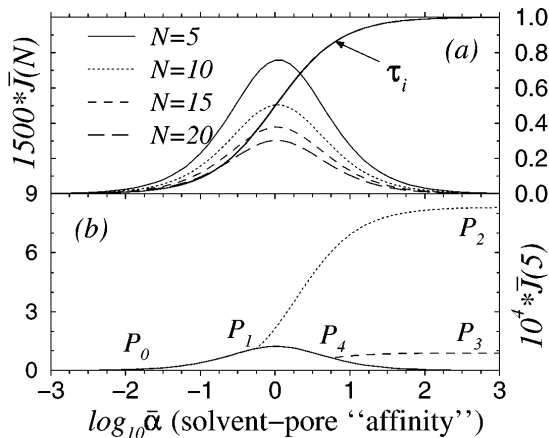


FIG. 2. (a) $1.5 \times 10^3 \bar{J}(N, \bar{\alpha})$ for $\Delta = 0.02$ and fixed $\bar{p}_0 = 1.0$. Various lengths are indicated. The solid curve between 0 and 1 is the average occupation number of any site. On this scale, the difference $\tau_1 - \tau_N$ is not apparent but varies qualitatively as \bar{J} . (b) The solid curve is $10^4 \times \bar{J}(5)$ for fixed $\bar{p}_0 = 0.1$. See text for explanation of curves $P_0 P_1 P_2$ and $P_0 P_1 P_4 P_3$.

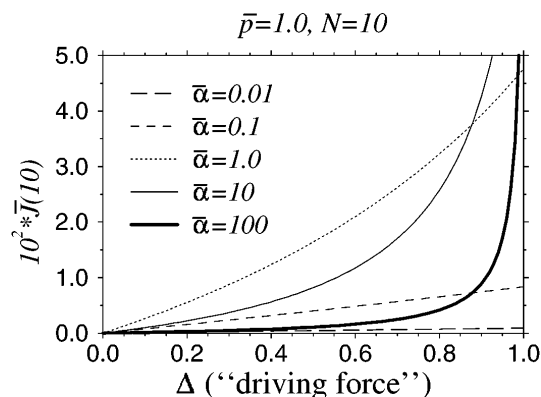


FIG. 3. Nonlinear behavior of $10^2 \times \bar{J}(10)$ for $\bar{p} = 1.0$ as a function of $\bar{\alpha}$. Note the competition between nonlinearities in $\bar{\alpha}$ and Δ , particularly at large Δ .

and averaging over one period, $\bar{J}(N) \simeq \bar{J}(N, \Delta_1 = 0) + c_2 \Delta_1^2$ where

$$c_2 = \begin{cases} \frac{\bar{\alpha}^2 \Delta_1^2}{2\bar{\alpha}(2 - \Delta_0) + 2}, & \bar{p} \gg (\bar{\alpha} + 1)N, \\ \frac{\Delta_1^2}{2(1 - \Delta_0)^2}, & \bar{p} \ll (\bar{\alpha} + 1)N, \end{cases} \quad (11)$$

for $\Delta_1/\Delta_0 \ll 1$. In the $\bar{p} \gg (\bar{\alpha} + 1)N$ limit, the temperature dependence of the flux enhancement is $-2E_\alpha/k_B T$ or $-E_\alpha/k_B T$, while the second limit is temperature independent. Electrostriction and mechanical deformation of the pores can also affect $\bar{\alpha}$ and therefore p via r_p [6].

In conclusion, modifications and extensions to the presented applications can be straightforwardly made. For example, effects of temperature differences, $T^{(R)} - T^{(L)} \neq 0$ can be readily extracted from (3). Furthermore, effects of internal-pore defects, such as those arising in (i) Gramicidin A, composed of two joined barrels, each in opposite lipid bilayer leaflets, (ii) lipid bilayers, with possible stiff unsaturated bonds along the aliphatic chains where molecules permeate, and (iii) zeolites, with interconnected cages and joints, can be calculated. If a pore has $N_p(N^*)$ junctions (independent of spatial distribution) with quenched hopping rates $p(p_k^*)$, the flux is given by (2) if N is replaced by $N_p + \sum_{k=1}^{N^*} (p/p_k^* - 1)$. This result is also an exact solution to the Heisenberg spin chain Hamiltonian with boundary conditions determined by $\{\mu\}$ and quenched random energies [12]. Osmosis experiments on Gramicidin A/bilayer liposomes reveal rich temperature dependences which are interpreted as lipid phase transitions inducing changes in how the Gramicidin A barrels are joined [13]. Actual flow measurements are ensemble averages over macroscopic membrane regions containing many pores: $\langle \bar{J} \rangle = \sum_{N, N^*, p^*} f(N, N^*, p_k^*) \bar{J}(N, N^*, p_k^*)$, where d is the membrane thickness, $N_{\min} \simeq d/\ell$, and $f(N, N^*, p_k^*)$ is the distribution of channels with arc-length $L = N\ell$, number of defects N^* , and defect strengths p_k^* . Finally, effects of unstirred or polarization layers (present only in osmo-

sis) near the pore mouths can be treated with a macroscopic convection-diffusion equation which yields an implicit equation $\bar{J} \propto \Delta(\bar{J})$ [11].

We have presented an exact nonlinear model of microporous transport valid when excluded particle volume contributions to the free energy dominate. The main results are a correspondence between microscopic interactions and macroscopic permeabilities defined by (6), (7), and their corresponding $k_B T$ dependences. Furthermore, we delineate cases where $\bar{J}(\bar{\alpha})$ has a maximum, represented by Fig. 2, and find nontrivial r_p dependences. Since relationships among the various kinetic parameters can be determined by equilibrium measurements such as solvent-solute heats and volumes of mixing, the simple model presented along with the numerous applicable physical systems offers a framework for experimental tests and will lead to a better understanding of more complex systems, including multispecies transport and chemical reactions in pores.

The author thanks E. B. and A. B. Kolomeisky, D. Lohse, T. J. Pedley, and A. E. Hill for comments and the Wellcome Trust for financial support.

- [1] V. Gupta, S. S. Nivarthi, A. V. McCormick, H. T. Davis, Chem. Phys. Lett. **247**, 596 (1995); K. Hahn, J. Kärger, and V. Kukla, Phys. Rev. Lett. **76**, 2762–2765 (1996).
- [2] A. Finkelstein, *Water Movement Through Lipid Bilayers, Pore, and Plasma Membranes* (Wiley-Interscience, New York, 1987); B. Alberts, D. Bray, and J. Lewis, *Molecular Biology of the Cell* (Garland, New York, 1994).
- [3] R. M. Barrer, *Zeolites and Clay Minerals as Sorbents and Molecular Sieves* (Academic Press, London, 1978).
- [4] K. Jirage, J. Hulteen, and C. Martin, Science **278**, 655 (1997).
- [5] S. Murad, Adsorption **2**, 95 (1996); S. Nivarthi, A. V. McCormick, and H. T. Davis, Chem. Phys. Lett. **229**, 297 (1994); V. Kukla, J. Kornatowski, D. Demuth, I. Girnus, H. Pfeifer, L. Rees, S. Schunk, K. Unger, and J. Kärger, Science **272**, 702 (1996).
- [6] S. Yashonath and P. Santikary, J. Phys. Chem. **98**, 6338 (1994).
- [7] J. Koplik, J. R. Banavar, and J. F. Willemsen, Phys. Fluids A **1**, 781 (1989); R. F. Cracknell, D. Nicholson, and N. Quirke, Phys. Rev. Lett. **74**, 2463–2466 (1995).
- [8] R. B. Stinchcombe and G. M. Schültz, Phys. Rev. Lett. **75**, 140 (1995); *Nonequilibrium Statistical Mechanics in One Dimension*, edited by V. Privman (Cambridge University Press, Cambridge, England, 1997).
- [9] M. Schreckenberg, A. Schadschneider, K. Nagel, and N. Ito, Phys. Rev. E **51**, 2939 (1995); K. Nagel and M. Paczuski, Phys. Rev. E **51**, 2909 (1995).
- [10] H. T. Davis, J. Chem. Phys. **93**, 4339 (1990); J. Piasecki and L. Peliti, J. Phys. A **26**, 4819 (1993).
- [11] T. Chou (to be published).
- [12] S. Sandow, Phys. Rev. E **50**, 2660 (1994).
- [13] B. A. Boehler, J. de Gier, and L. L. M. van Deenen, Biochim. Biophys. Acta **512**, 480–488 (1978).